Journal of Hydrometeorology

Snow Ablation over the Western United States Mountains: Patterns and Controlling Factors

--Manuscript Draft--

Manuscript Number:	JHM-D-19-0198
Full Title:	Snow Ablation over the Western United States Mountains: Patterns and Controlling Factors
Article Type:	Article
Corresponding Author:	Mu Xiao University of California Los Angeles Los Angeles, CA UNITED STATES
Corresponding Author's Institution:	University of California Los Angeles
First Author:	Mu Xiao
Order of Authors:	Mu Xiao
	Sarith P. Mahanama
	Yongkang Xue
	Fei Chen
	Dennis P. Lettenmaier
Abstract:	Snow accumulation over the mountainous Western U.S. is usually reasonably well predicted by widely-used hydrological models. However, there is a much greater divergence among otherwise “good” models in their simulation of snow ablation process. Here, we explore differences in the performance of VIC, Noah-MP, Catchment and SSiB3 in their ability to reproduce observed snow water equivalent (SWE) during the ablation season at ten SNOTEL stations with over 20 years of record. During the ablation period net radiation generally has stronger correlations with observed melt rates than does air temperature. Average ablation rates tend to be higher (in both model predictions and observations) at stations with large accumulated SWE, where the snowpack remains on average as the downward solar radiation approaches its seasonal peak. Of the four models, VIC and Noah-MP simulate higher net radiation with a larger portion allocated to canopy upward sensible heat (i.e., heat flux from the surface to the overlying air). In Catchment and SSiB3, the sensible heat tends to be downward during the ablation period which enhances the melt energy. If we manually change the surface cover to bare soil in all the models, the magnitude of sensible heat in VIC and Noah-MP decreases dramatically, as in these two models a large portion of the sensible heat flux during the snow season comes from canopy. Catchment predicts decreased sensible heat under the bare soil situation, as it does not include attenuation of wind speed in its calculation and removing the canopy only reduces the surface roughness.
Suggested Reviewers:	Jessica Lundquist jdlund@uw.edu
	Kelly Elder Kelly.j.elder@usda.gov
	Danny Marks danny.marks@ars.usda.gov
	Youlong Xia youlong.xia@noaa.gov
	Jeff Dozier dozier@ucsb.edu

UNIVERSITY OF CALIFORNIA, LOS ANGELES UCLA

BERKELEY · DAVIS · IRVINE · LOS ANGELES · RIVERSIDE · SAN DIEGO · SAN FRANCISCO

SANTA BARBARA · SANTA CRUZ

Dennis P. Lettenmaier
Geography Department, Box 91524
Los Angeles, CA. 90095-1524
Email: dlettenm@ucla.edu phone: 310-794-4327

August 6, 2019

Dr. Wade T. Crow
Chief Editor, *Journal of Hydrometeorology*
American Meteorological Society
45 Beacon St.
Boston, MA 02108

Dear Wade:

RE: "Snow Ablation over the Western United States Mountains: Patterns and Controlling Factors " by Xiao et al.

We are submitting the referenced manuscript for review by *JHM*. The paper evaluates the performance of the snow algorithms in four widely used hydrology/land surface models during the ablation period, using a set of observation stations (NRCS/SnoTel) distributed across the Western U.S.

This manuscript describes original work and is not under consideration by any other journal.

We suggest as possible reviewers:
Jessica Lundquist jdlund@uw.edu
Jeff Dozier dozier@ucsb.edu
Kelly Elder Kelly.j.elder@usda.gov
Danny Marks danny.marks@ars.usda.gov
Youlong Xia youlong.xia@noaa.gov

I will serve as the paper's corresponding author.

Sincerely

Dennis P. Lettenmaier, NAE
Distinguished Professor of Geography

Snow Ablation over the Western United States Mountains: Patterns and Controlling Factors

Mu Xiao[1], Sarith P. Mahanama[2,3], Yongkang Xue[1], Fei Chen[4] and Dennis P. Lettenmaier[1]

[1]Department of Geography, University of California, Los Angeles, CA

[2]Global Modeling and Assimilation Office, NASA GSFC, Greenbelt, MD

[3]Science Systems and Applications, InC., Lanham, MD

[4]Research Application Laboratory, National Center for Atmospheric Research, Boulder, CO

Corresponding author: Dennis P. Lettenmaier, dlettenm@ucla.edu

Abstract

Snow accumulation over the mountainous Western U.S. is usually reasonably well predicted by widely-used hydrological models. However, there is a much greater divergence among otherwise "good" models in their simulation of snow ablation process. Here, we explore differences in the performance of VIC, Noah-MP, Catchment and SSiB3 in their ability to reproduce observed snow water equivalent (SWE) during the ablation season at ten SNOTEL stations with over 20 years of record. During the ablation period net radiation generally has stronger correlations with observed melt rates than does air temperature. Average ablation rates tend to be higher (in both model predictions and observations) at stations with large accumulated SWE, where the snowpack remains on average as the downward solar radiation approaches its seasonal peak. Of the four models, VIC and Noah-MP simulate higher net radiation with a larger portion allocated to canopy upward sensible heat (i.e., heat flux from the surface to the overlying air). In Catchment

and SSiB3, the sensible heat tends to be downward during the ablation period which enhances the melt energy. If we manually change the surface cover to bare soil in all the models, the magnitude of sensible heat in VIC and Noah-MP decreases dramatically, as in these two models a large portion of the sensible heat flux during the snow season comes from canopy. Catchment predicts decreased sensible heat under the bare soil situation, as it does not include attenuation of wind speed in its calculation and removing the canopy only reduces the surface roughness.

1.0 Introduction

Snow is a dominant aspect of the land surface hydrological cycle of the Western U.S., especially in the headwaters of the major river basins. Snowpacks store precipitation during the cold season and release water via melt during the following warm season, effectively providing a natural reservoir that shifts the timing of peak runoff relative to precipitation by several months. In most Western U.S. river basins, snow is the largest (seasonally varying) water storage component (Mote et al. 2005). Li et al. (2017) found that 53% of the runoff over the Western U.S. originates from melting snowpacks, a number that increases to 70% in the mountainous parts of the region. In relatively dry and heavily-populated Southern California, more than half the water supply is derived from snowmelt from remote mountainous sources (Waliser et al. 2011). As temperatures have warmed in recent decades, snowpack behavior and corresponding hydrological processes have been severely affected. For instance, Mote et al. (2018) report that over 90% of the snow monitoring stations across the Western U.S. with long-term records have shown declines over 1955-2014. As temperatures continue to warm, Rauscher et al. (2008) estimate that snowmelt-driven runoff over the West could occur as much as two months earlier than it has historically.

Despite its importance to surface water hydrology, determining representations of the complicated mechanisms that govern snowpack accumulation and ablation in hydrologic models remain challenging. Given both the scientific challenges and practical implications, Dozier et al. (2016) have argued that estimation of the spatial distribution of SWE over mountainous areas is the most important unsolved issue in snow hydrology. The problem is complicated by the fact that snow depth variability can be caused by a mix of multiple process at various spatial scales

(Clark et al. 2011). On the other hand, snow accumulation over the Western U.S. is usually well predicted by the accumulated precipitation occurring during the winter at temperatures below a threshold (typically slightly greater than 0˚C on daily average). For instance, Figure 1(a) shows that SWE estimated using a very simple rule that approximates the seasonal maximum SWE as the accumulation of all precipitation that occurs during the winter season below a fixed (daily average) temperature predicts maximum winter snow accumulations reasonably accurately. Figure 1 also shows that different land surface models reproduce observed SWE maxima that are reasonably close to the observations over the Western U.S. Where there is a much greater divergence among otherwise "good" models is in their predictions of snow ablation. Figure 1(c) shows, when the models are initialized with the observed seasonal SWE maxima, the variations in ablation rates are substantial, and can lead to variations in the predicted date of last SWE that exceed one month.

Here, we explore, in off-line simulations, the ablation season performance of four energy-based snow models that are widely used in macroscale hydrologic models and coupled land-atmosphere models. In particular, we examine their ability to reproduce observed snow ablation rates at selected Snow Telemetry (SNOTEL) sites (snow pillows operated by Natural Resources Conservation Service (NRCS)) across the Western U.S. We examine differences among the snow models (and between models and observations) during the ablation period by analyzing a range of factors that control snow ablation. The remainder of the paper is organized as the follows: section 2 describes the data and models used in the comparisons. We report results in section 3, with interpretation and discussion in section 4. Finally, our conclusions are presented in section 5.

2.0 Data and Methods

2.1 Snow observations and ablation estimate

The USDA Natural Resources Conservation Service (NRCS) Snow Survey and Water Supply Forecasting (SSWSF) Program (https://www.wcc.nrcs.usda.gov/) has a network of more than 750 automated SNOTEL stations in the Western States. Starting in the early 1980s, the SNOTEL stations began to report daily snow water equivalent (SWE) using snow pillows (which essentially weigh the accumulated snowpack continuously in time), as well as (most sites) daily precipitation, and daily maximum and minimum temperature. We selected 10 SNOTEL stations distributed over the Western United States (Figure 2) whose data are of high quality (missing values less than 5%). These stations form the basis for our analyses. The station names and elevations are given in Table 1.

In order to evaluate snow ablation characteristics, we first need to define the ablation process and melt rates. Dyer and Mote (2007) defined a snow ablation event as a period with a decrease in snow depth between two successive days. They assessed trends in ablation events over North America accordingly. However, our focus does not require such a short temporal scale, as our main objectives are to explore the behavior and the controlling factors during the (entire) snow melt season and to determine the bias and uncertainty among the models in estimating SWE during this period. Therefore, we use a broader definition of the ablation period, which is: for each water year (Oct-Sep), the ablation period is the time from the date of maximum SWE to the last day of snow existence (SWE>0). Further, we extract the 20th-80th-quantile of the ablation period, which we define as the period from the date when 80% of the maximum accumulated SWE remains to the date when 20% of SWE remains. Based on our exploratory analysis, focusing

on this central portion of the melt period seems to provide a representation of the ablation process that is free from unusual conditions near the beginning and end of the melt period (e.g., occasional accumulation events early in the melt period, and very warm conditions with partial snow cover late in the melt period). We performed some comparisons (not reported) that showed that our results were not very sensitive to modest changes in our definition of the ablation period. Therefore, In the analyses we report below, our results are based on the 20th-80th-quantile definition unless stated otherwise. Accordingly, we calculate snow ablation rates for each year the 80th-quantile of SWE minus the 20th-quantile of SWE divided by the number of days between the corresponding dates.

2.2 Land surface models

We examined simulations of SWE using four Land Surface Models (LSMs) : Variable Infiltration Capacity (VIC), Noah Multi-Parameterization (Noah-MP), Catchment, and Simplified SiB version 3 (SSiB3), all of which have been applied previously in numerous snow-related studies (e.g. Tan et al. 2011; Shi et al. 2013; Chen et al. 2014; Newman et al. 2014; Xia et al. 2016; Magand et al. 2013; Xue et al. 2018; Oaida et al. 2015; and Cortés et al. 2016 among many others). The relevant archival references for the snow algorithms in the four models are: VIC (Andreadis et al. 2009); Noah-MP (Niu et al. 2011); Catchment (Stieglitz et al. 2001); and SSiB3 (Sun et al. 1999; Xue et al. 2003). The key features of the snow algorithms in each of the model are summarized in Table 2. We also provide brief descriptions of each model below.

VIC is a physical-based, macroscale hydrologic model with an energy-based snow module that explicitly accounts for snow accumulation and ablation in the vegetation canopy (Liang and Lettenmaier 1994; Andreadis et al. 2009). It represents two layers in the vertical (one for thin

snowpacks) – a relatively thin surface layer, and a deeper pack layer. The VIC snow model is capable of simulating sub-grid variability in vegetation canopies and the effects of topography on snow accumulation and ablation via "tile" and elevation band representations, respectively. It also has a parameterization for subgrid redistribution of SWE (e.g., via wind).

Noah-MP has much different physics than the original Noah LSM (Chen and Dudhia 2001; Ek et al. 2003) to the extent that it essentially is a different model. Regarding the snowpack modeling, the Noah-MP snow model partitions the snowpack into up to three layers according to the snow depth and snow cover fraction as determined by snow density, snow depth and ground roughness length. Within each grid cell, Noah-MP utilizes a "semi-tile" scheme to calculate the energy balance and solves for the snow temperature over the vegetated and bare fractions separately.

Catchment incorporates a three-layer snow module to account for snowpack growth and ablation (Stieglitz et al. 2001). Catchment determines the net solar radiation flux using estimates of surface albedo; this albedo is calculated separately for the snow-covered and snow-free fractions of the land element, and vegetation "sticking out" of the snowpack modifies the albedo in the snow-covered fraction. The model calculates the heat flow within the snowpack via linear diffusion, with thermal conductivity a function of snow density. Snow can melt in the upper snow layers and, following percolation, can refreeze in lower layers. Snowmelt water that leaves the snowpack either infiltrates the soil or is removed from the system as runoff. Turbulent fluxes into the air (including sublimation) are determined as part of the energy balance calculations performed for the top (~8 cm) snow layer. Catchment redistributes the heat contents and mass of snow into the three layers at every time step. Catchment does not separate downward solar

radiation according to vegetated and bare-soil surfaces, i.e. it does not use a two-stream scheme as do other three models. Instead, it would first calculate the tile-average surface albedo (with and without snow) and compute the net solar radiation for the entire tile.

SSiB3 uses the snow-atmosphere-soil transfer (SAST) model of Sun et al. (1999). SAST uses up-to three layers to represent snow in vegetation-free areas and under forest canopies. Each tile is divided into canopy and bare soil partitions according to the vegetation fraction in the same way that SSiB does for snow-free tiles. The snow energy fluxes and surface soil temperature are solved simultaneously to guarantee energy conservation at each time step.

2.3 Forcings and experimental set-up

We extracted daily meteorological observations (daily precipitation and temperature maxima and minima) at the selected SNOTEL sites. We used wind speed from the Livneh data set (Livneh et al. 2013) which is interpolated from the lowest layer of the NCEP/NCAR reanalysis (Kalnay et al. 1996). We applied the Mountain Climate (MTCLIM) algorithms (Hungerford et al. 1989) as incorporated in the VIC model (Bohn et al. 2013) at each station to produce hourly downward solar and longwave radiation, pressure and humidity forcings. Our study period is from 1991 to 2012, which was determined by the availability of the SNOTEL meteorological observations and the temporal coverage of the Livneh dataset.

To evaluate the magnitude and nature of differences in ablation rates among the models, we manually adjusted the SWE predictions for all models to match the SNOTEL annual maxima for each water year (i.e. within every year, when the SNOTEL observation reached its annual maximum, we replaced the simulated SWE on that day with the observed value). We then continued the model simulations through the date of last snow, and repeated the process for the

next water year. This procedure allowed us to focus entirely on the models' predictions of snow ablation, without confounding them with differences in snow accumulation.

3.0 Results

3.1 Ablation rates

Figure 3 shows the average ablation rates calculated as described in section 2.1 at each of the 10 SNOTEL sites for the 21-year study period 1992-2012. Overall, the Catchment model produced the best estimates as compared with observations in terms of Mean Absolute Error (MAE). SSiB had slightly higher MAEs than Catchment. VIC and Noah-MP both generally had melt rates that were biased low with one or two exceptions (e.g. site 10 for VIC, sites 7 and 9 for Noah-MP), where the estimated ablation rates exceeded those from observations by up to 105%. The overall bias across all models is slightly negative (the observations have higher ablation rates than the simulations) although SSiB has generally positive biases. The multi-model ensemble-average yielded melt rates with MAEs that were slightly higher than the best model. The station-averaged errors (model minus observed) in the estimated last day of the ablation period are 9.3 (VIC), 3.6 (Noah-MP), -1.6 (SSiB), -0.1 (Catchment) and 2.8 (model-average) days, respectively.

Table 3 summarizes the climatologies of the 10 SNOTEL sites in terms of average temperature and maximum annual SWE. Considering the ablation rates in Figure 3 and the maximum SWE values in the table, the stations that have the highest SWE accumulations also tend to experience faster melt rates. Figure 4 reports the correlation coefficients between average annual maximum SWE and average ablation rates for the observations and modeled results across all 10 stations. Linear regression relationships are also plotted in the figure. The results from observations are highly correlated (r=0.97) as are the Catchment results. Only VIC is

an outlier with a (relatively) small r-value of 0.78. One possible reason to explain the correlations is that the low SWE stations melt their snow before the period of highest available energy (late spring and early summer). As the downward solar radiation increases seasonally, only those stations with higher SWE remain snow covered. The snowpack at these high SWE stations receives more downward shortwave radiation later in the year, and thus tends to have higher ablation rates. Musselman et al. (2017) argue that in a warmer climate, snow ablation rates in the western U.S. will decrease for this reason, which is generally consistent with our results.

3.2 Dependence on temperature and net-radiation

Figure 5 shows the results of linear regressions of the computed ablation rates on the average temperature during the melt season along with the correlation coefficients for observed and simulated results. Overall, the correlations between ablation and temperature are high, with values from observations ranging from 0.51 to 0.92 with an average of 0.73. The model results also show more or less linear dependences, with only 10% of the r-values across all stations and models less than 0.6). Although there are some deviations for individual models, the model-averaged results in general capture the observed relationships between temperature and ablation rates at each of the SNOTEL sites.

Figure 6 is similar to Figure 5, except with temperature replaced with net radiation. There is no observation-based net-radiation, instead we used the average net radiation from the four LSMs as a surrogate for observations. The correlation coefficients in Figure 6 generally are higher than in Figure 5. In particular, the station average for both observation-based (0.92 in the last subplot of Fig 6) and model-averaged (0.94 in the last subplot of Fig 6) both are substantially higher than those in Figure 5 (0.73 for observed analysis and 0.81 for model average). Statistically,

63.6% of the r-values in Figure 5 are greater than 0.8, and this percentage increases to 78.8% in the Figure 6 net-radiation correlation results. This result should not be surprising as net radiation is the dominant source of melt energy, and temperature appears only in the net longwave radiation component of net radiation (which generally is much smaller than net shortwave during the melt season). This result is consistent with Painter et al. (2018) who show, in the different context of the role of dust on snowmelt rates that radiative forcings are a much more important determinant of snowmelt rates that cause the rising limb of the hydrograph in Upper Colorado's spring runoff than is temperature. One could in fact argue that the only reason that the temperature correlations in Figure 5 are as high as they are is that high temperatures tend to be correlated with clear sky conditions during the melt period, which in turn are associated with high downward solar radiation.

We also performed a similar test of the relationship between wind speed and ablation rate. We found that correlations were weak in most cases. Only three SNOTEL sites have statistically significant ($p<0.05$) correlations between wind speed and ablation rate (Figure S0). At those three sites, there is a (weak) inverse relationship between net-radiation and wind speed, which likely leads to the apparent relationship with wind speed. We do note that the source of our wind speed data is the surface level wind in the NCEP-NCAR reanalysis (Kalnay et al. 1996) which is a coarse scale product (2.5 degrees latitude by longitude) which is unable to capture local scale variations in wind speed. However, a larger factor likely is that wind speed is a determinant of turbulent fluxes (latent and sensible heat) which generally are of opposite sign during the ablation period, and therefore tend to be small in magnitude relative to net radiation. During rain-on-snow events (which do occur occasionally during the ablation period) latent heat

flux can be an important contributor to melt (Moore and Owens 1984; Guan et al. 2016). However, such events occur infrequently enough, and are of small enough magnitude during the melt period, that they appear not to have a major effect on ablation.

4.0 Discussion

4.1 Energy components

To better understand the factors that control snowmelt, we need to identify the sources of melt energy. The surface energy budget equation (which is represented directly in all four of the LSMs), can be expressed as:

$$Q_M = Rn + SH + LH + GH + Q_A,$$

where Q_M is the energy absorbed by the snowpack (melt energy), Rn is the net radiation, SH is the sensible heat flux, LH is the latent heat flux, GH is the ground heat flux, and Q_A is the energy advected to the snowpack by precipitation (the directions of these energy terms in the equation are all downward). GH and Q_A are usually small during the melt season and we neglect them. We focus here on Rn, SH, LH, and their residual Qr (Rn + SH + LH) which accounts for most of the melt energy.

We show simulated net radiation, sensible heat and latent heat fluxes for each model and station in Figure 7. Net shortwave, net longwave and net downward radiation are shown in Figure 8. In Figure 7, the white circles indicate Qr, the melt energy. VIC and Noah-MP exhibit similar behaviors, with large negative sensible heat during the ablation period (i.e. the surface warms the air) except for VIC at Schofield Pass (site 10). SSiB and Catchment generally have positive sensible heat fluxes, which means that energy is transferred from the air to the surface. Having upward sensible heat flux over snow-covered site in the forest is not unrealistic, as shown by

ground observations reported a previous study (Fig.9 in Chen et al. 2014). Of the four models, Noah-MP produces the most net radiation. However, its ablation rate is not the highest, as it also has large negative sensible heat flux. Generally, SSiB has the largest melt energy Qr, and hence it produces the highest ablation rates among the models. However, we also note that there are few exceptions where these relationships among models are reversed, e.g. Noah-MP vs SSiB at site 7 and site 9, which implies that SSiB may be allocating more energy to ground heat flux there.

4.2 Vegetation effects

During the ablation process, if present, the vegetation canopy, can play an important role in energy transfer to the snowpack. Furthermore, each model determines the vegetation cover types on computational surface tiles on their own way using various global data sets etc. Usually (although not always, see below) SNOTEL sites are located in clearings surrounded with at most short vegetation that is covered by snow for most of the ablation season. Each model's vegetation cover mechanism is distinct as is its representation of the interaction between canopy and land surface and snow on and under vegetation. For example, VIC uses pre-defined sub-tiles to represent different types of canopy cover and the final result is an area-weighted average (Liang et al., 1994). Noah-MP utilizes a dynamic vegetation cover fraction, which is related to the LAI value (Niu et al. 2011). In Catchment, each computational tile is assigned a single vegetation type and the overall surface albedo of the tile is then determined as the weighted average of snow free and snow-covered fractions. Catchment's snow free parameterization is designed to match MODIS climatological mean albedo at the location at any given time. The snow parameterization in Catchment (Stieglitz et al. 2001) uses a 13 mm threshold of SWE to compute the snow-covered fraction within the tile, i.e. if SWE is greater than or equal to 13 mm, the entire

tile is assumed to be snow covered. SSiB employs a monthly-varying parameters for vegetation cover fraction, leaf area index, and other vegetation properties dependent on vegetation type (Sellers et al. 1996).

Furthermore, the models have different representations of how much snow can be intercepted by the vegetation canopy and the energetics of snow on and below the canopy. Their representations of the effects of the canopy on absorption and re-radiation of solar radiation, as well as the effects of the canopy on wind, and hence under-canopy turbulent fluxes also vary. Arguably the first consideration (snow interception) is less important during the ablation season than is the second (vegetation effects on under-canopy net radiation and turbulent fluxes.

In order to evaluate the canopy effects and corresponding model behaviors, we performed a parallel set of simulations, whose setup was the same as the baseline described above but with the vegetation cover removed. For comparison purposes, we give the vegetation type of each model and some key vegetation parameters for the baseline simulation in Table 4.

Figure 9 shows the ablation rates that resulted from the no vegetation experiment (note that the melt rates calculated from the observations are identical to the results shown in Figure 3 as they require no assumptions about vegetation). From Figure 9, we see that without the canopy cover, the ablation rate in Noah-MP increases substantially. VIC's response is similar in direction but the magnitude of the changes is much smaller. Melt rates for both Catchment and SSiB are reduced relative to their baseline runs when the vegetation is removed. Overall, removal of vegetation results in large degradation of Noah-MP's performance relative to observations (MAE increases to 17.0 mm/day from 6.7 mm/day in the baseline experiment). VIC and SSiB have smaller MAEs in the no canopy condition relative to the baseline. The MAE of Catchment

increases very slightly in the no vegetation simulation (likely because the baseline simulation assumes only short vegetation; see Table 4). We do note that at some of the sites (Olallie Meadows, Banner Summer, Blue Mountain Spring, and Silver Creek in particular) a review of photos of the SNOTEL sites shows the presence of some vegetation in the vicinity of the snow pillow, i.e., the no vegetation assumption may not be entirely appropriate. In those cases, the no vegetation assumption is best interpreted as an end point for comparison with the vegetated base runs.

To explain the cause and effect of different model behaviors, we need to analyze the energy components in the no vegetation simulations and relate them to the models' own algorithms. Figure 10 shows the energy terms and Figure 11 presents the breakdown of tile-wide net radiation (net shortwave and net longwave) for all models from the no vegetation simulations. The downward net longwave radiation decreases in the no vegetation scenario for all models (24.6% averaged over the four models), as removing the canopy eliminates the contribution of longwave re-radiated from the canopy (which originates as solar radiation absorption). The net shortwave radiation in VIC, Noah-MP and SSiB all decrease in the no vegetation experiment while Catchment shows a slight increase. We explore the causes of Catchment's behavior below.

In Catchment, the overall net shortwave and net longwave radiation consists of two parts: energy from snow-covered and non-snow parts of each tile. When the SWE in Catchment is greater than 13 mm (which is almost always true during our 20-80-quantile ablation period), the model considers the tile to be fully snow covered and applies the snow surface albedo to the entire tile. The simulated net shortwave and net longwave are almost identical when it is fully covered by snow (as Figure 12 shows). However, the vegetation substantially affects Catchment's

calculation of sensible heat. Vegetation cover increases the surface roughness and thus decreases the aero-dynamic resistance. With no wind attenuation effect, removing the canopy decreases the surface roughness and thus reduces the sensible heat. Therefore, the snowpack receives more melt energy and the ablation period becomes shorter in the no vegetation experiment. The reduced snow season leads to less net radiation during ablation, because the snowpack is gone before most of the seasonal increase in downward solar radiation increases (as Figure 11 and Figure 12 shows).

The Rn, SH and LH terms show different responses to canopy removal as Figure 10 indicates. Compared to the baseline experiment, the overall behaviors of Qr (defined in section 4.1; as indicated by the white marker on the bars) are that VIC and Noah-MP experience increases, whereas SSiB and Catchment decrease, consistent with the ablation rate responses of each model. It is worth noting that all the sensible heat flux terms are positive for each model in the no vegetation experiment, i.e. heat is being transferred from the air to the snowpack in this situation. In the presences of canopy cover, VIC and Noah-MP have negative (upward) sensible heat fluxes (which means the tile is warming the air) as shown in Figure 7. Although VIC and Noah-MP can absorb more energy in the baseline experiments (with vegetation), a large portion of that absorbed energy (41.7% in VIC and 42.5% in Noah-MP) is distributed to heat the air and hence not to melt snow (the behaviors of sensible heat flux in VIC and Noah-MP is further explored below). In the no vegetation experiment, although the net radiation in VIC and Noah-MP is reduced, the sensible heat switches from negative to positive and the overall effect leads to more melt energy.

VIC and Noah-MP represent wind attenuation effects on under-canopy turbulent heat fluxes. Therefore, it is somewhat counter-intuitive that the sensible heat fluxes in both models decrease substantially in the no vegetation experiment. The reason of this behavior is that the vegetation component of sensible heat dominates total sensible heat flux in both models when vegetation is present (total sensible = sensible from canopy + sensible from ground). Figures S1 and S2 show time-series of the sensible heat components (canopy and ground) during the ablation season for both models. In the no vegetation experiment, the sensible heat from the snow surface does in fact increase in both models relative to under-canopy sensible heat when vegetation is present (the increase is larger in VIC than Noah-MP). But the increase is much too small to cancel the loss of sensible heat from the canopy, which of course isn't present in the no vegetation experiments. When vegetation is present, the trees would absorb energy and transfer much more heat to the air, which is the main contributor of sensible heat. Therefore, the overall magnitude would decrease if we remove canopy cover in VIC and Noah-MP.

All the models follow the general rule that the snow albedo is greater than that of bare soil and vegetation cover. Therefore, if we remove the canopy in the simulation, the net downward shortwave radiation decreases in VIC, Noah-MP and SSiB as Figures 8 and 11 show. The only exception is the Catchment model, which treats the entire tile as fully covered by snow when SWE is greater than 13 mm and employs snow albedo to calculate absorbed solar energy (as we have discussed above).

5 Summary and Conclusions

We employed four widely used energy-based LSM snow models in offline simulations to explore differences in melt season ablation rates at 10 SNOTEL stations across the Western

United States. We extracted precipitation and temperature data from in-situ observations at each of the SNOTEL sites. We manually adjusted the maximum annual SWE value each year to match the in-situ observations for the purpose of focusing on differences in model performance during the ablation periods. We assessed the linear dependence of the ablation rate on two major atmospheric factors: temperature and radiation. We also performed a no vegetation scenario to study the effects of vegetation on ablation rates at each of the SNOTEL sites. Based on these experiments, we conclude that:

1) On average, the four LSMs produce ablation rates that match observations at the SNOTEL sites in the baseline experiments plausibly well. The average MAE for all models is 4.3 mm/day (22% of the observed average ablation rate across the 10 stations), ranging from 3.6 mm/day (Catchment) to 6.7 mm/day (Noah-MP). SSiB is the only model that has positive bias (higher ablation rate than observations) in the baseline experiments. The multi-model average of the estimated last day of the ablation period has a bias of about half a week (last day of snow on average 2.8 days later than in observations). In experiments where we removed the canopy cover, the MAE values averaged over models becomes 34% of the observed station-average ablation rate. The MAE of each individual model in the no-vegetation simulations is close to the baseline results: SSiB has a tiny improvement while VIC and Catchment produce slightly higher values. One model (Noah-MP) is an exception; it has a large increase in MAE in the no-vegetation scenario.
2) The modeled ablation rates are highly correlated with accumulated maximum SWE in part because high SWE stations have their ablation periods at a time of year (generally later in spring than low SWE sites) when downward solar radiation, and hence net radiation, is

higher. Net radiation is highly correlated with ablation rates (more so than is temperature), which is consistent with other published studies. Wind speed is not a strong predictor of ablation rates during the melting process.

3) The effects of vegetation canopy cover vary substantially across the models. The presence of a vegetation canopy increases the average ablation rates in two models (VIC and Noah-MP), but decreases ablation in SSiB and Catchment. When the canopy is removed, the simulated sensible heat reverses direction and its magnitude decreases substantially (in absolute value) in VIC and Noah-MP. The direction of sensible heat is unchanged in Catchment and SSiB, but the magnitude of the former decreases and of the the latter increases. The difference among models is attributable to changes with removal of vegetation in the fate of absorbed solar energy (due to lower albedo relative to the snowpack) of vegetation, surface albedo representations, parameterizations of the attenuation of wind speed by canopies, and how much of the absorbed radiation is transformed to sensible heat (which warms the air) as contrasted with re-radiated longwave (much of which becomes melt energy). The differences in model parameterizations that lead to these inter-model differences in vegetation effects should be a topic for further development in the modeling community.

Acknowledgement

References:

Andreadis, K. M., P. Storck, and D. P. Lettenmaier, 2009: Modeling snow accumulation and ablation processes in forested environments. *Water Resour. Res.*, **45**, 1–13, doi:10.1029/2008WR007042.

Bohn, T. J., B. Livneh, J. W. Oyler, S. W. Running, B. Nijssen, and D. P. Lettenmaier, 2013: Global evaluation of MTCLIM and related algorithms for forcing of ecological and hydrological models. *Agric. For. Meteorol.*, **176**, 38–49, doi:10.1016/j.agrformet.2013.03.003. http://dx.doi.org/10.1016/j.agrformet.2013.03.003.

Chen, F., and J. Dudhia, 2001: Coupling an Advanced Land Surface–Hydrology Model with the Penn State–NCAR MM5 Modeling System. Part I: Model Implementation and Sensitivity. *Mon. Weather Rev.*, **129**, 569–585, doi:10.1175/1520-0493(2001)129<0569:CAALSH>2.0.CO;2. http://journals.ametsoc.org/doi/abs/10.1175/1520-0493%282001%29129%3C0587%3ACAALSH%3E2.0.CO%3B2.

——, and Coauthors, 2014: Modeling seasonal snowpack evolution in the complex terrain and forested colorado headwaters region: A model intercomparison study. *J. Geophys. Res.*, **119**, 13795–13819, doi:10.1002/2014JD022167.

Clark, M. P., and Coauthors, 2011: Representing spatial variability of snow water equivalent in hydrologic and land-surface models: A review. *Water Resour. Res.*, **47**, doi:10.1029/2011WR010745.

Cortés, G., M. Girotto, and S. Margulis, 2016: Snow process estimation over the extratropical Andes using a data assimilation framework integrating MERRA data and Landsat imagery.

Water Resour. Res., **52**, 2582–2600, doi:10.1002/2015WR018376. http://doi.wiley.com/10.1002/2015WR018376.

Dozier, J., E. H. Bair, and R. E. Davis, 2016: Estimating the spatial distribution of snow water equivalent in the world's mountains. *Wiley Interdiscip. Rev. Water*, **3**, 461–474, doi:10.1002/wat2.1140. http://doi.wiley.com/10.1002/wat2.1140.

Dyer, J. L., and T. L. Mote, 2007: Trends in snow ablation over North America. *Int. J. Climatol.*, **27**, 739–748, doi:10.1002/joc.1426. http://cdiac.esd.ornl.gov/oceans/GLODAP/glodap_pdfs/Thermohaline.web.pdf.

Ek, M. B., K. E. Mitchell, Y. Lin, E. Rogers, P. Grunmann, V. Koren, G. Gayno, and J. D. Tarpley, 2003: Implementation of Noah land surface model advances in the National Centers for Environmental Prediction operational mesoscale Eta model. *J. Geophys. Res.*, **108**, 8851, doi:10.1029/2002JD003296. http://doi.wiley.com/10.1029/2002JD003296.

Guan, B., D. E. Waliser, F. M. Ralph, E. J. Fetzer, and P. J. Neiman, 2016: Hydrometeorological characteristics of rain-on-snow events associated with atmospheric rivers. *Geophys. Res. Lett.*, **43**, 2964–2973, doi:10.1002/2016GL067978.

Hungerford, R. D., R. R. Nemani, S. W. Running, and J. C. Coughlan, 1989: MTCLIM: a mountain microclimate simulation model. doi:10.2737/INT-RP-414. https://www.fs.usda.gov/treesearch/pubs/39815.

Kalnay, E., and Coauthors, 1996: The NCEP/NCAR 40-Year Reanalysis Project. *Bull. Am. Meteorol. Soc.*, **77**, 437–471, doi:10.1175/1520-0477(1996)077<0437:TNYRP>2.0.CO;2. http://journals.ametsoc.org/doi/abs/10.1175/1520-0477%281996%29077%3C0437%3ATNYRP%3E2.0.CO%3B2.

Li, D., M. L. Wrzesien, M. Durand, J. Adam, and D. P. Lettenmaier, 2017: How much runoff originates as snow in the western United States, and how will that change in the future? *Geophys. Res. Lett.*, **44**, 6163–6172, doi:10.1002/2017GL073551. http://doi.wiley.com/10.1002/2017GL073551.

Liang, X., and D. Lettenmaier, 1994: a simple hydrologically based model of land surface water and energy fluxes for general circulation models. *J. Geophys. …*, **99**. http://onlinelibrary.wiley.com/doi/10.1029/94JD00483/full (Accessed April 16, 2014).

Livneh, B., E. A. Rosenberg, C. Lin, B. Nijssen, V. Mishra, K. M. Andreadis, E. P. Maurer, and D. P. Lettenmaier, 2013: A long-term hydrologically based dataset of land surface fluxes and states for the conterminous United States: Update and extensions. *J. Clim.*, **26**, 9384–9392, doi:10.1175/JCLI-D-12-00508.1. http://journals.ametsoc.org/doi/abs/10.1175/JCLI-D-12-00508.1 (Accessed October 22, 2014).

Magand, C., A. Ducharne, N. Le Moine, and S. Gascoin, 2013: Introducing Hysteresis in Snow Depletion Curves to Improve the Water Budget of a Land Surface Model in an Alpine Catchment. *J. Hydrometeorol.*, **15**, 631–649, doi:10.1175/jhm-d-13-091.1.

Moore, R. D., and I. F. Owens, 1984: Controls on Advective Snowmelt in a Maritime Alpine Basin. *J. Clim. Appl. Meteorol.*, **23**, 135–142, doi:10.1175/1520-0450(1984)023<0135:coasia>2.0.co;2.

Mote, P. W., A. F. Hamlet, M. P. Clark, and D. P. Lettenmaier, 2005: Declining Mountain Snowpack in Western North America*. *Bull. Am. Meteorol. Soc.*, **86**, 39–49, doi:10.1175/BAMS-86-1-39.

——, S. Li, D. P. Lettenmaier, M. Xiao, and R. Engel, 2018: Dramatic declines in snowpack in the

western US. *npj Clim. Atmos. Sci.*, **1**, 2, doi:10.1038/s41612-018-0012-1. http://www.nature.com/articles/s41612-018-0012-1.

Musselman, K. N., M. P. Clark, C. Liu, K. Ikeda, and R. Rasmussen, 2017: Slower snowmelt in a warmer world. *Nat. Clim. Chang.*, doi:10.1038/nclimate3225.

Newman, A. J., M. P. Clark, A. Winstral, D. Marks, and M. Seyfried, 2014: The Use of Similarity Concepts to Represent Subgrid Variability in Land Surface Models: Case Study in a Snowmelt-Dominated Watershed. *J. Hydrometeorol.*, **15**, 1717–1738, doi:10.1175/JHM-D-13-038.1. http://journals.ametsoc.org/doi/abs/10.1175/JHM-D-13-038.1.

Niu, G. Y., and Coauthors, 2011: The community Noah land surface model with multiparameterization options (Noah-MP): 1. Model description and evaluation with local-scale measurements. *J. Geophys. Res. Atmos.*, **116**, 1–19, doi:10.1029/2010JD015139.

Oaida, C. M., Y. Xue, M. G. Flanner, S. M. Skiles, F. De Sales, and T. H. Painter, 2015: Improving snow albedo processes in WRF/SSiB regional climate model to assess impact of dust and black carbon in snow on surface energy balance and hydrology over western U.S. *J. Geophys. Res. Atmos.*, **120**, 3228–3248, doi:10.1002/2014JD022444. http://doi.wiley.com/10.1002/2014JD021636.

Painter, T. H., S. M. K. Skiles, J. S. Deems, W. T. Brandt, and J. Dozier, 2018: Variation in Rising Limb of Colorado River Snowmelt Runoff Hydrograph Controlled by Dust Radiative Forcing in Snow. *Geophys. Res. Lett.*, **45**, 797–808, doi:10.1002/2017GL075826.

Rauscher, S. A., J. S. Pal, N. S. Diffenbaugh, and M. M. Benedetti, 2008: Future changes in snowmelt-driven runoff timing over the western US. *Geophys. Res. Lett.*, **35**, 1–5, doi:10.1029/2008GL034424.

Sellers, P. J., C. J. Tucker, G. J. Collatz, S. O. Los, C. O. Justice, D. A. Dazlich, and D. A. Randall, 1996: A Revised Land Surface Parameterization (SiB2) for Atmospheric GCMS. Part II: The Generation of Global Fields of Terrestrial Biophysical Parameters from Satellite Data. *J. Clim.*, **9**, 706–737, doi:10.1175/1520-0442(1996)009<0706:ARLSPF>2.0.CO;2. http://journals.ametsoc.org/doi/abs/10.1175/1520-0442%281996%29009%3C0706%3AARLSPF%3E2.0.CO%3B2.

Shi, X., S. J. Déry, P. Y. Groisman, and D. P. Lettenmaier, 2013: Relationships between recent pan-arctic snow cover and hydroclimate trends. *J. Clim.*, **26**, 2048–2064, doi:10.1175/JCLI-D-12-00044.1. http://journals.ametsoc.org/doi/abs/10.1175/JCLI-D-12-00044.1.

Stieglitz, M., A. Ducharne, R. Koster, and M. Suarez, 2001: The Impact of Detailed Snow Physics on the Simulation of Snow Cover and Subsurface Thermodynamics at Continental Scales. *J. Hydrometeorol.*, **2**, 228–242, doi:10.1175/1525-7541(2001)002<0228:TIODSP>2.0.CO;2.

Sun, S., J. Jin, and Y. Xue, 1999: A simple snow-atmosphere-soil transfer model. *J. Geophys. Res.*, **104**, 587–597.

Tan, A., J. C. Adam, and D. P. Lettenmaier, 2011: Change in spring snowmelt timing in Eurasian Arctic rivers. *J. Geophys. Res.*, **116**, D03101, doi:10.1029/2010JD014337.

Waliser, D., and Coauthors, 2011: Simulating cold season snowpack: Impacts of snow albedo and multi-layer snow physics. *Clim. Change*, **109**, 95–117, doi:10.1007/s10584-011-0312-5.

Xia, Y., D. Mocko, M. Huang, X. Cai, M. Rodell, K. E. Mitchell, M. B. Ek, and B. Li, 2016: Comparison and Assessment of Three Advanced Land Surface Models in Simulating Terrestrial Water Storage Components over the United States. *J. Hydrometeorol.*, **18**, 625–649, doi:10.1175/jhm-d-16-0112.1.

Xue, Y., S. Sun, D. S. Kahan, and Y. Jiao, 2003: Impact of parameterizations in snow physics and interface processes on the simulation of snow cover and runoff at several cold region sites. *J. Geophys. Res.*, **108**, 8859, doi:10.1029/2002JD003174. http://doi.wiley.com/10.1029/2002JD003174.

Xue, Y., B. A. Forman, and R. H. Reichle, 2018: Estimating Snow Mass in North America Through Assimilation of Advanced Microwave Scanning Radiometer Brightness Temperature Observations Using the Catchment Land Surface Model and Support Vector Machines. *Water Resour. Res.*, **54**, 6488–6509, doi:10.1029/2017WR022219.

Table 1: Site locations and attributes for the selected SNOTEL sites.

Site #	Station name	Lon	Lat	State	Elevation (m)
1	Olallie Meadows	-121.44	47.37	WA	1228
2	Hand Creek	114.84	48.31	MT	1535
3	Pike Creek	-113.33	48.30	MT	1808
4	Hemlock Butte	-115.63	46.48	ID	1771
5	Banner Summit	-115.23	44.30	ID	2146
6	Blue Mountain Spring	-118.52	44.25	OR	1789
7	Silver Creek	-121.18	42.96	OR	1750
8	Central Sierra Snow Laboratory	-120.37	39.33	CA	2101
9	Leavitt Lake	-119.61	38.28	CA	2194
10	Schofield Pass	-107.05	39.02	CO	3261

Table 2: Key features of the snow-related physics in the four Land Surface Models.

	VIC	Noah-MP	SSiB	Catchment
Snow albedo decay	Yes	Yes	Yes	Yes
Canopy interception	Liquid and snow	Liquid and snow	Liquid and snow	Liquid and snow
Canopy radiation transfer	Two streams	Two streams	Two streams	Tile average
Max snow layers	2-layer	3-layer	3-layer	3-layer
Canopy attenuation of solar radiation	Yes	No	Yes	Yes
Canopy attenuation of wind	Yes	Yes	Yes	No

Table 3: Climatology of average April-July daily temperature (T), annual maximum SWE and average temperature during ablation as defined in section 2.1 at selected stations over 1992-2012.

#	Station name	Avg Apr-Jul T (˚C)	Avg SWE (mm)	Avg T during melt period (˚C)
1	Olallie Meadows	7.3	1362.4	8.1
2	Hand Creek	8.7	272.8	4.6
3	Pike Creek	8.1	572.9	7.0
4	Hemlock Butte	8.8	1117.8	9.0
5	Banner Summit	7.4	614.6	6.5
6	Blue Mountain Spring	8.9	396.7	5.0
7	Silver Creek	9.7	293.9	3.8
8	Central Sierra Snow Laboratory	9.0	973.0	5.1
9	Leavitt Lake	6.1	314.6	8.2
10	Schofield Pass	5.4	910.9	6.5

Table 4: Vegetation cover type for the LSMs at the selected SNOTEL sites. The corresponding LAI are reported in Table S1.

#	Station name	VIC	Noah-MP	SSiB	Catchment
1	Olallie Meadows	Evergreen needleleaf and mixed cover	Evergreen Needleleaf	Needleleaf with ground cover	Ground cover
2	Hand Creek	Evergreen needleleaf and woodland	Evergreen Needleleaf	Evergreen needleleaf	Ground cover
3	Pike Creek	Evergreen needleleaf	Evergreen Needleleaf	Evergreen needleleaf	Ground cover
4	Hemlock Butte	Evergreen needleleaf and mixed cover	Evergreen Needleleaf	Needleleaf with ground cover	Ground cover
5	Banner Summit	Evergreen needleleaf, woodland and grasslands	Evergreen Needleleaf	Broadleaf shrubs with ground cover	Ground cover
6	Blue Mountain Spring	Woodland	Evergreen Needleleaf	Broadleaf shrubs with ground cover	Ground cover
7	Silver Creek	Woodland	Evergreen Needleleaf	Broadleaf shrubs with ground cover	Ground cover
8	Css Lab	Evergreen needleleaf, woodland and grasslands	Evergreen Needleleaf	Broadleaf shrubs with ground cover	Ground cover
9	Leavitt Lake	Evergreen needleleaf, woodland and grasslands	Evergreen Needleleaf	Dwarf trees with ground cover	Ground cover
10	Schofield Pass	Woodland and Grasslands	Mixed forest	Grassland	Ground cover

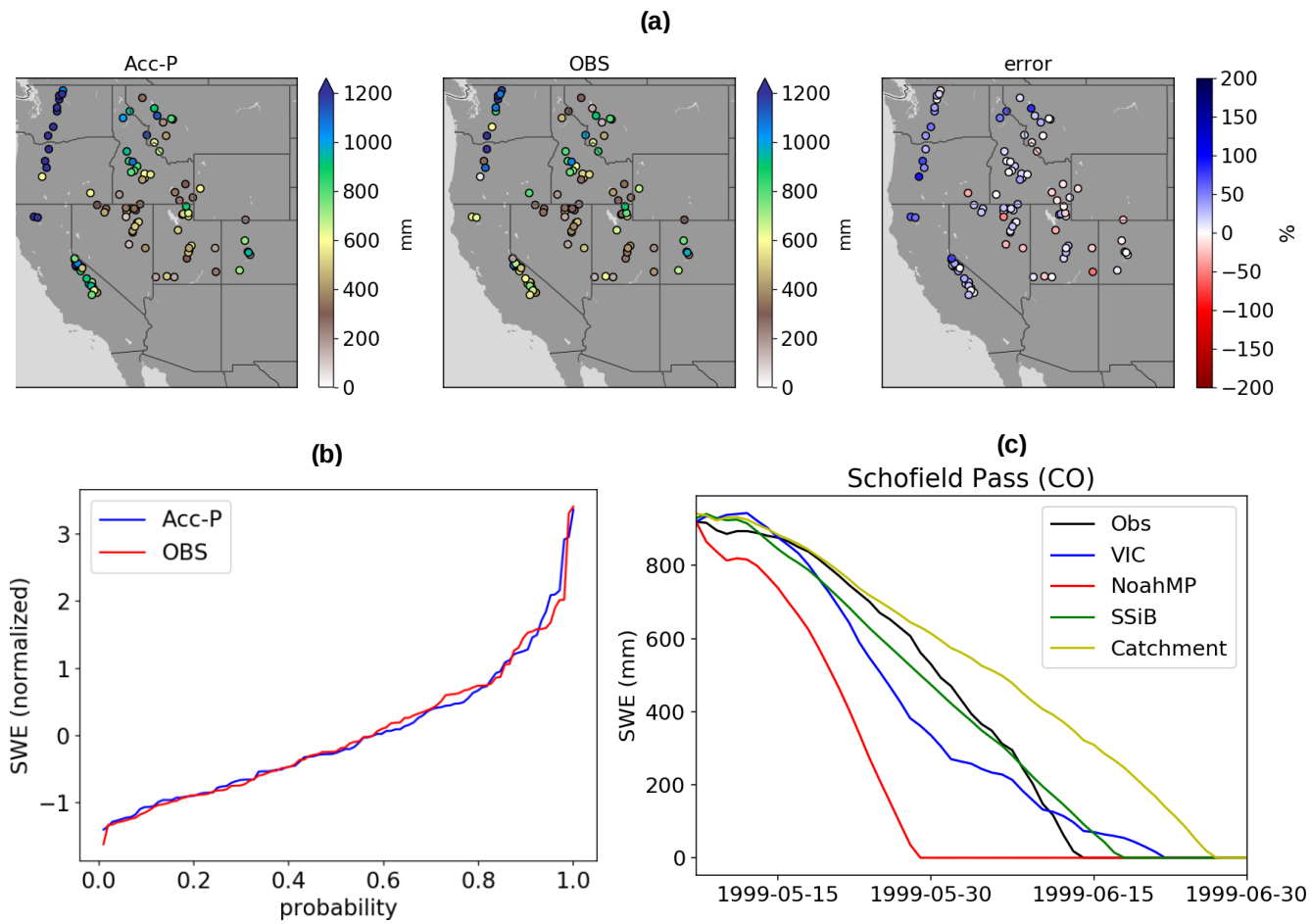

Figure 1: (a) Climatology of annual maximum SWE estimated by accumulated precipitation (Acc-P), observations (OBS) and error percentage over 1986-2005 averaged over ~100 SNOTEL stations. (b) Empirical cumulative probability curves for annual maximum SWE from observations (OBS) and accumulated precipitation (ACC-P) over all the stations in (a). Both the red and blue lines are normalized. (c) Observed and simulated SWE time-series plot for Schofield Pass, CO. The models are initialized with the observed annual maximum SWE.

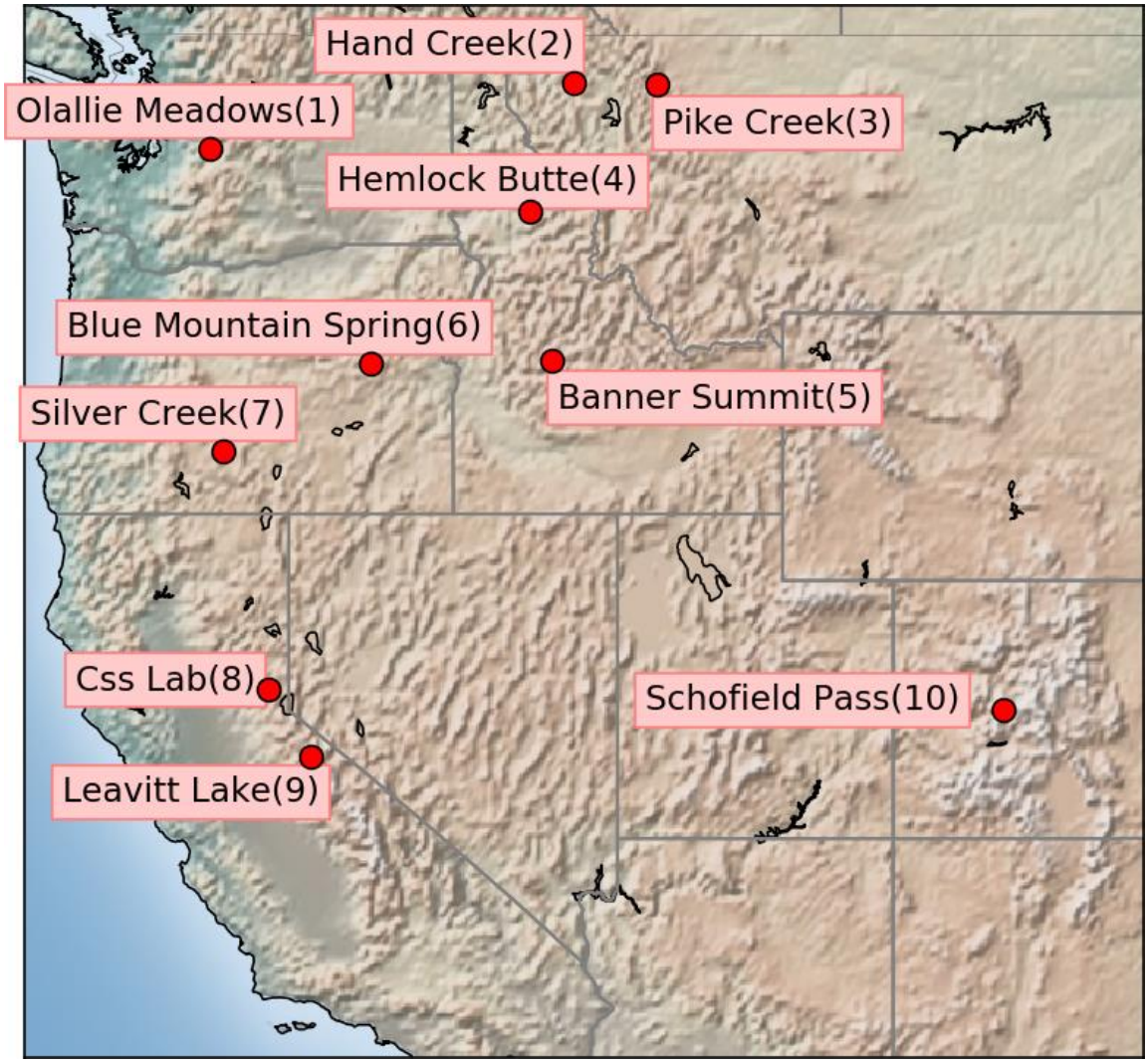

Figure 2: Selected NRCS SNOTEL stations over the Western U.S. The names and index numbers correspond to the information given in Table 1.

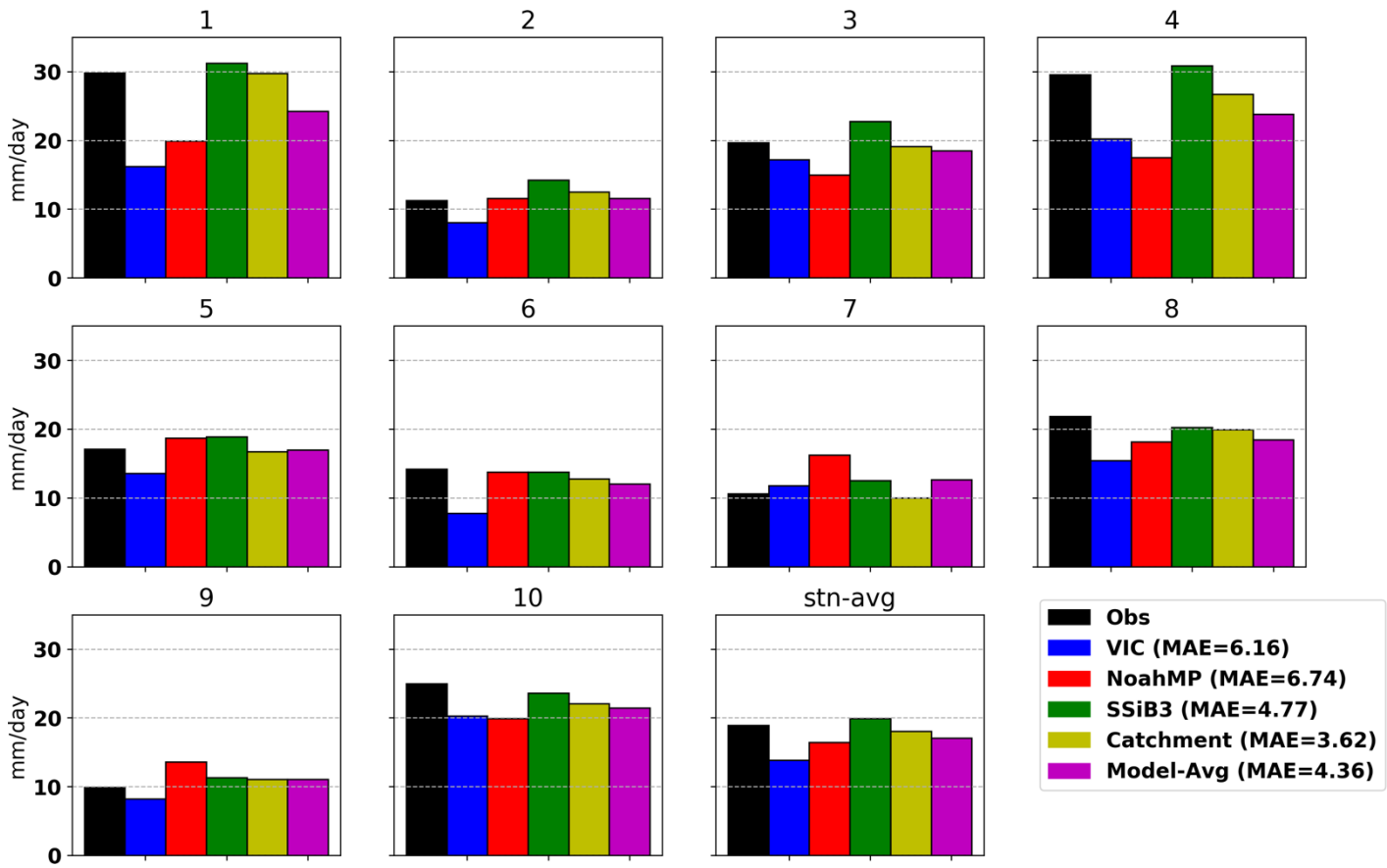

Figure 3: Snow ablation rates at the 10 SNOTEL sites averaged over 1992-2012 water years.

Index numbers correspond to Table 1; “stn-avg” is the mean over all stations.

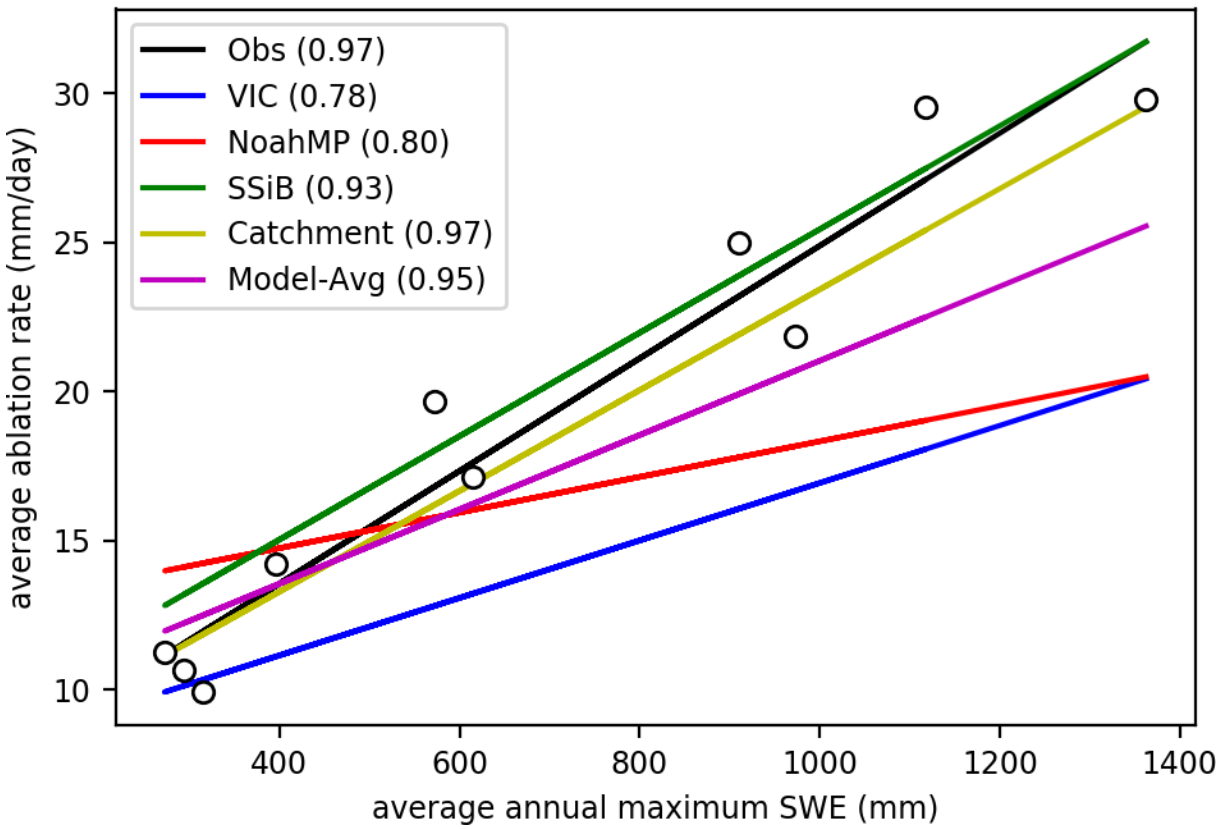

Figure 4: Linear regressions between annual maximum SWE climatology and average melt rates over the 10 sites. The legend provides the correlation coefficients. The circles are the mean observed melt rate vs mean observed SWE.

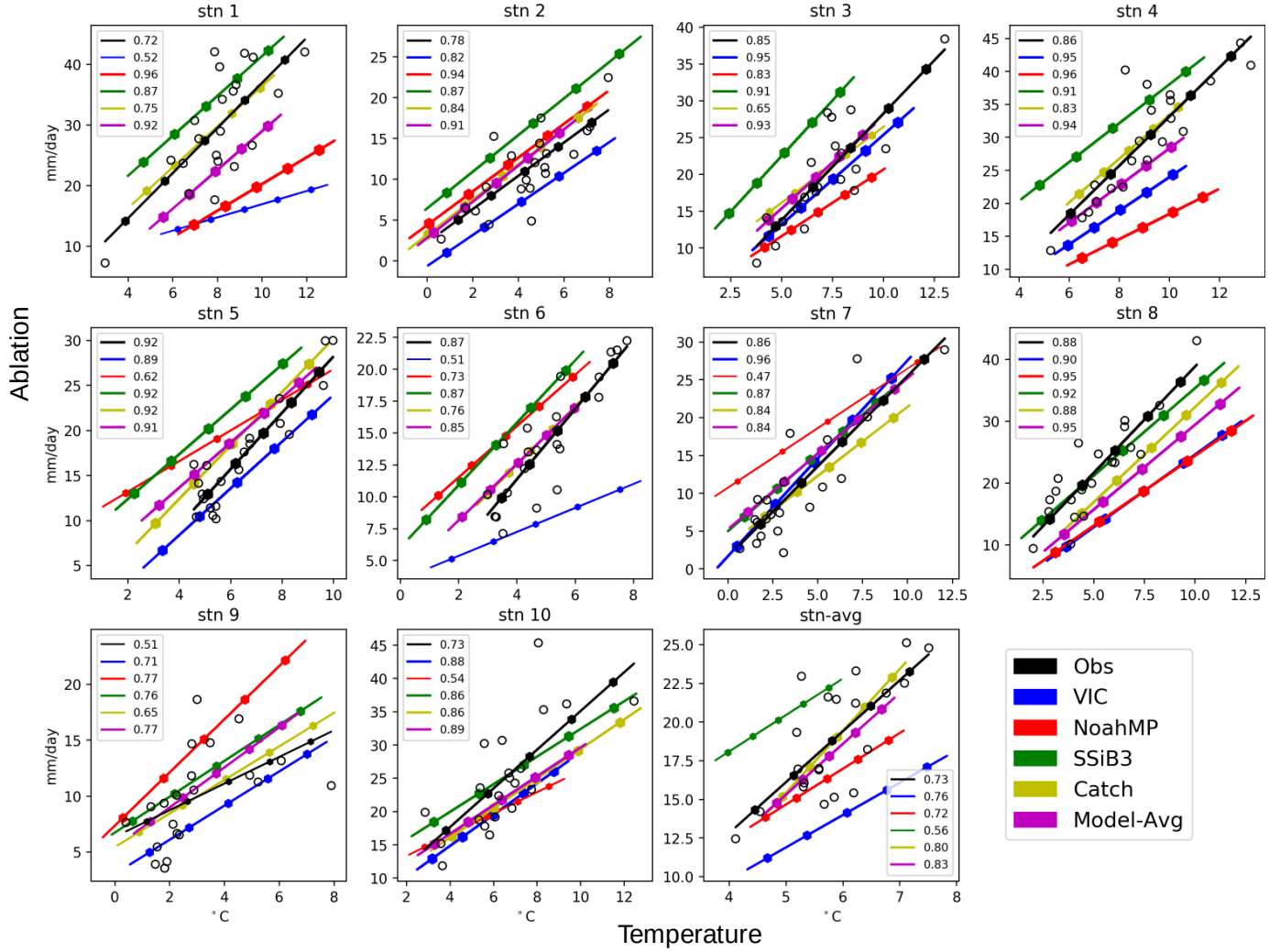

Figure 5: Linear regressions of melt rate against average temperature during the melt period across all stations for both observed and simulated data (correlation coefficients are given in the legend). The black circles are the observed ablation rates. The ablation units are mm/day (temperature in ˚C). Larger plot symbols indicate higher r-values.

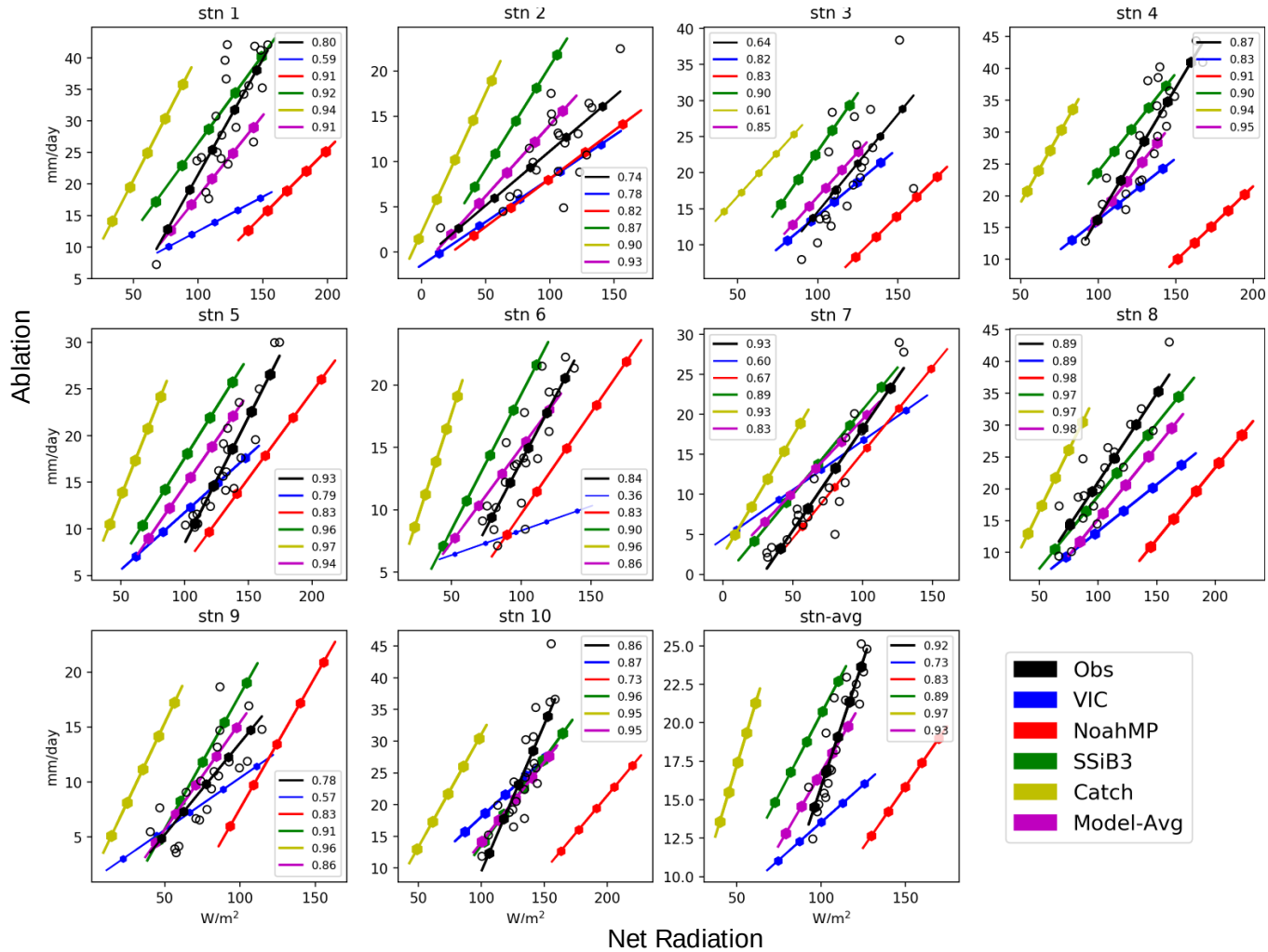

Figure 6: Same as Figure 5 but the temperature is replaced by net radiation. For the 'Obs' curves we use model-averaged net radiation as a surrogate for observations. Net radiation units are W/m^2.

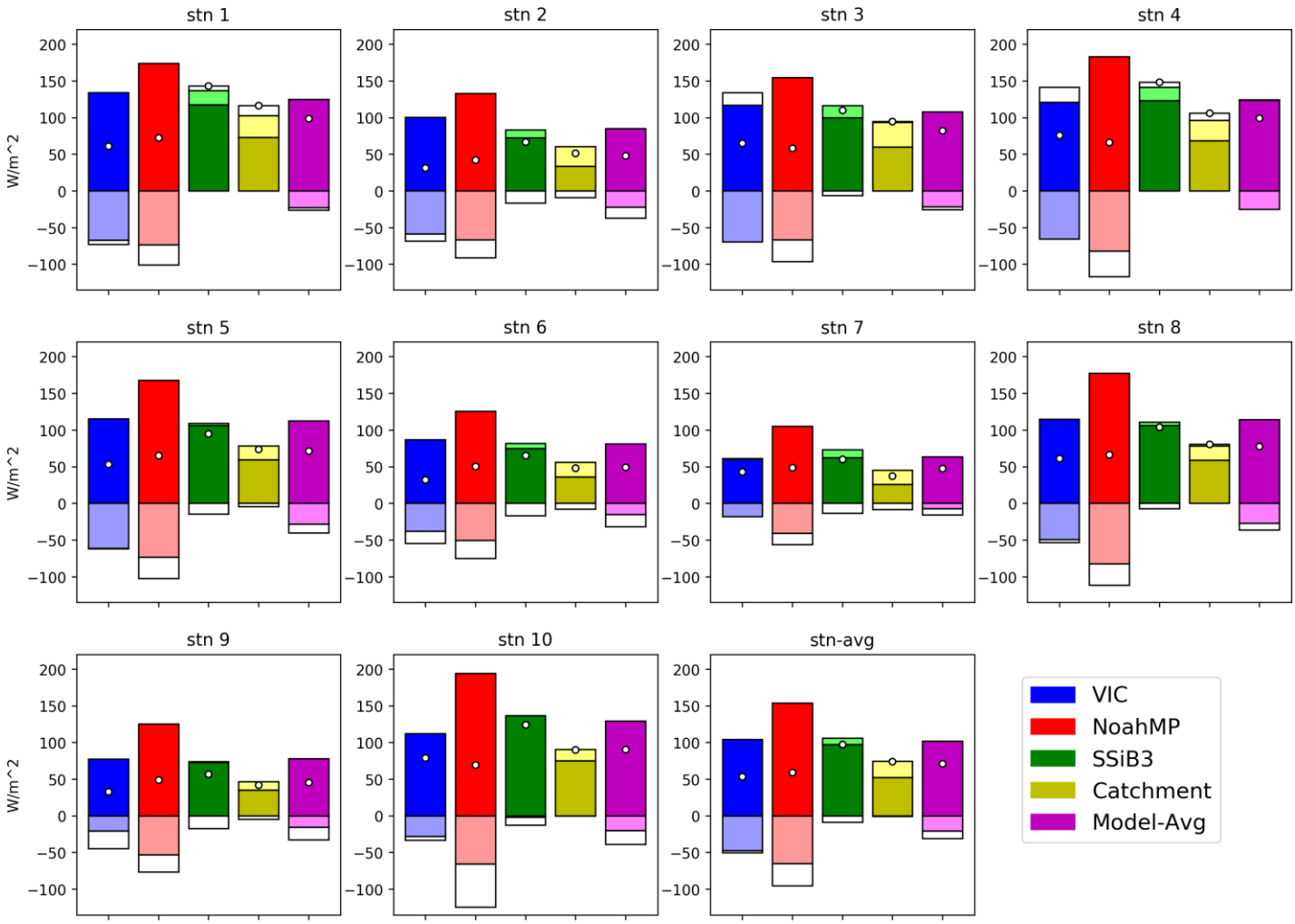

Figure 7: Energy components for each of the 10 SNOTEL stations. The deep colored bars indicate net radiation (Rn), the white bars are the latent heat (LH), and the shaded bars are the sensible heat (SH). The white dots indicate the energy difference term, Qr (Rn-LH-SH). All nits are W/m^2.

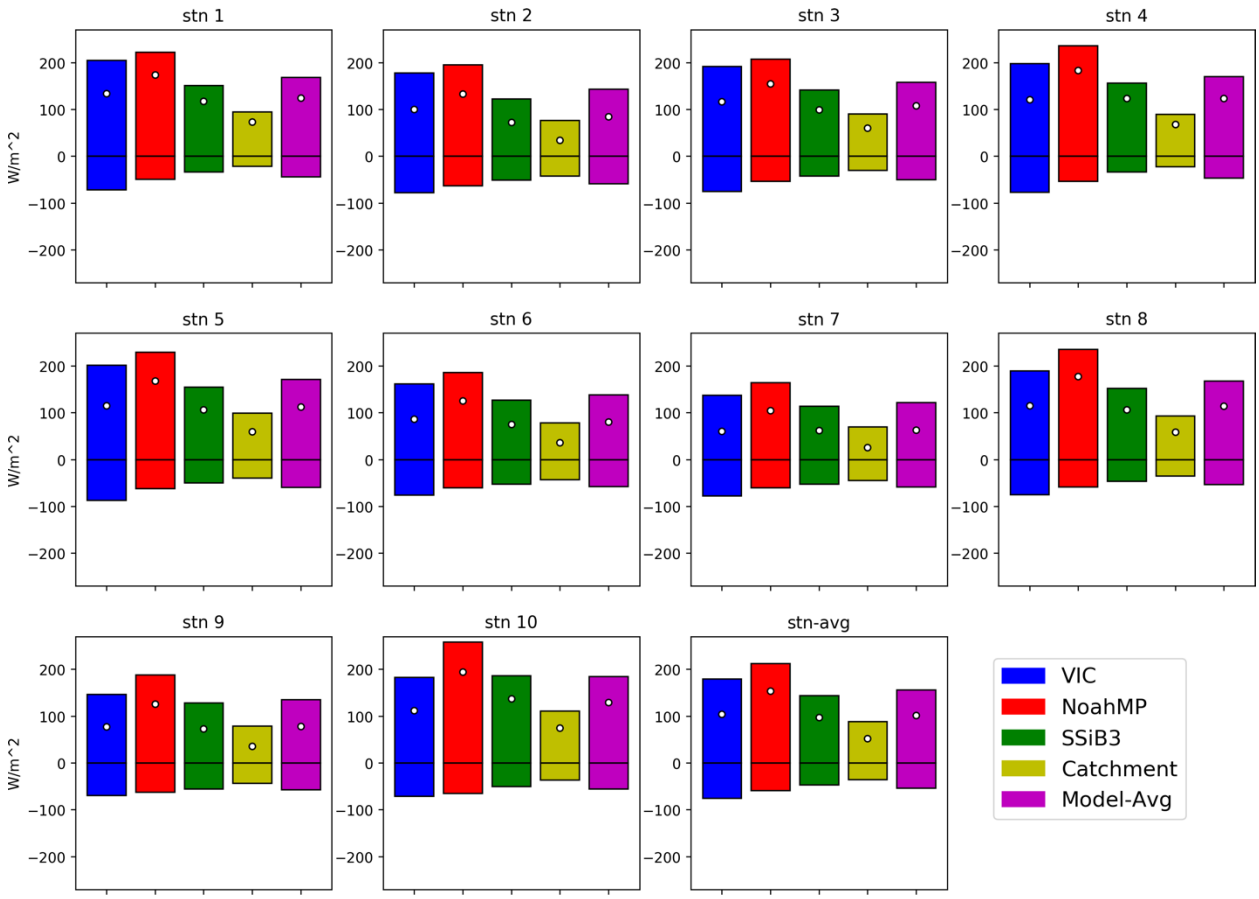

Figure 8: Tile-wide downward net shortwave (positive) and net longwave (negative) radiation in W/m^2 over all the SNTOEL sites. White circles indicate the net radiation (i.e. net shortwave minus net longwave) term.

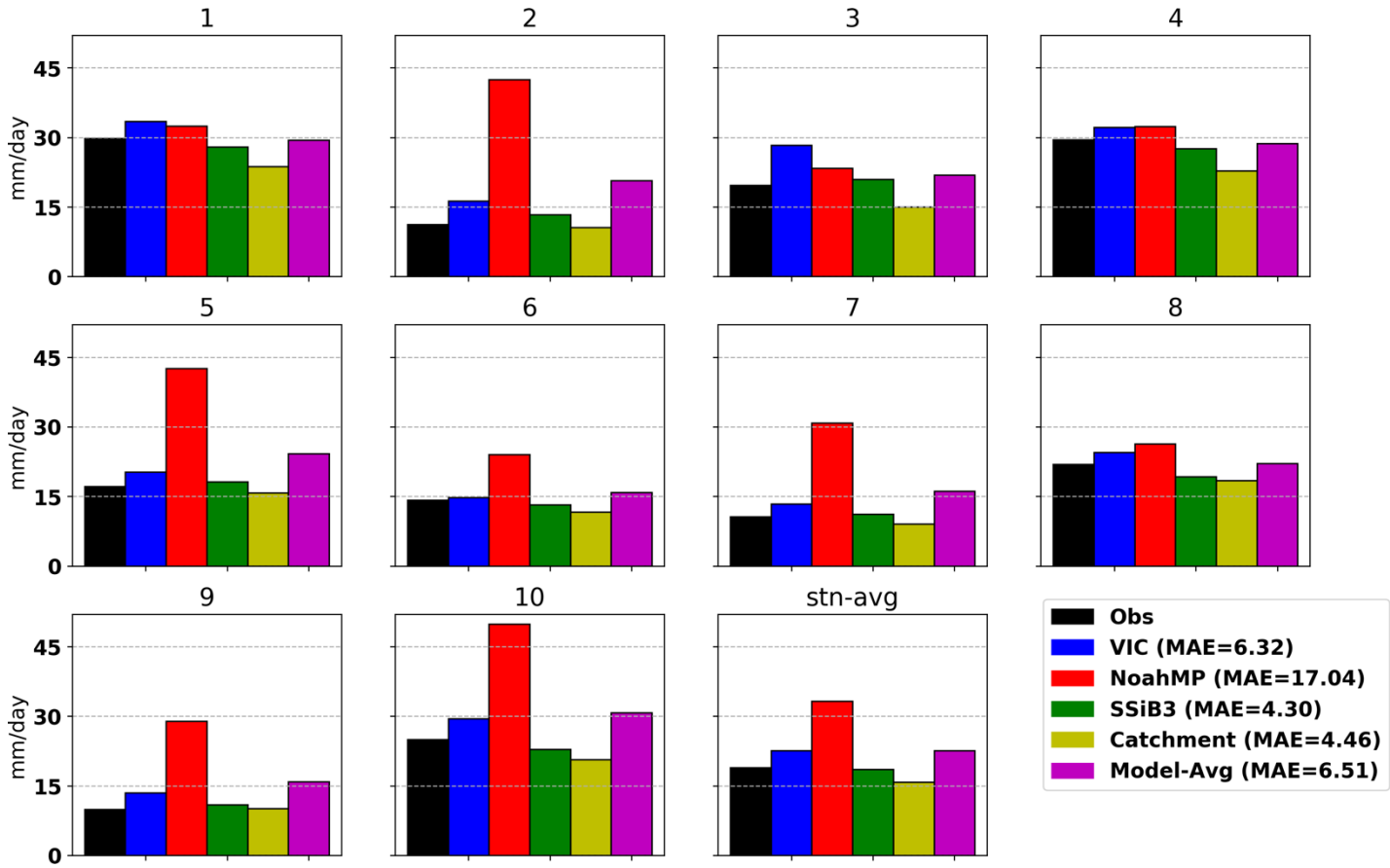

Figure 9: same as Figure 3 but for the no vegetation simulation.

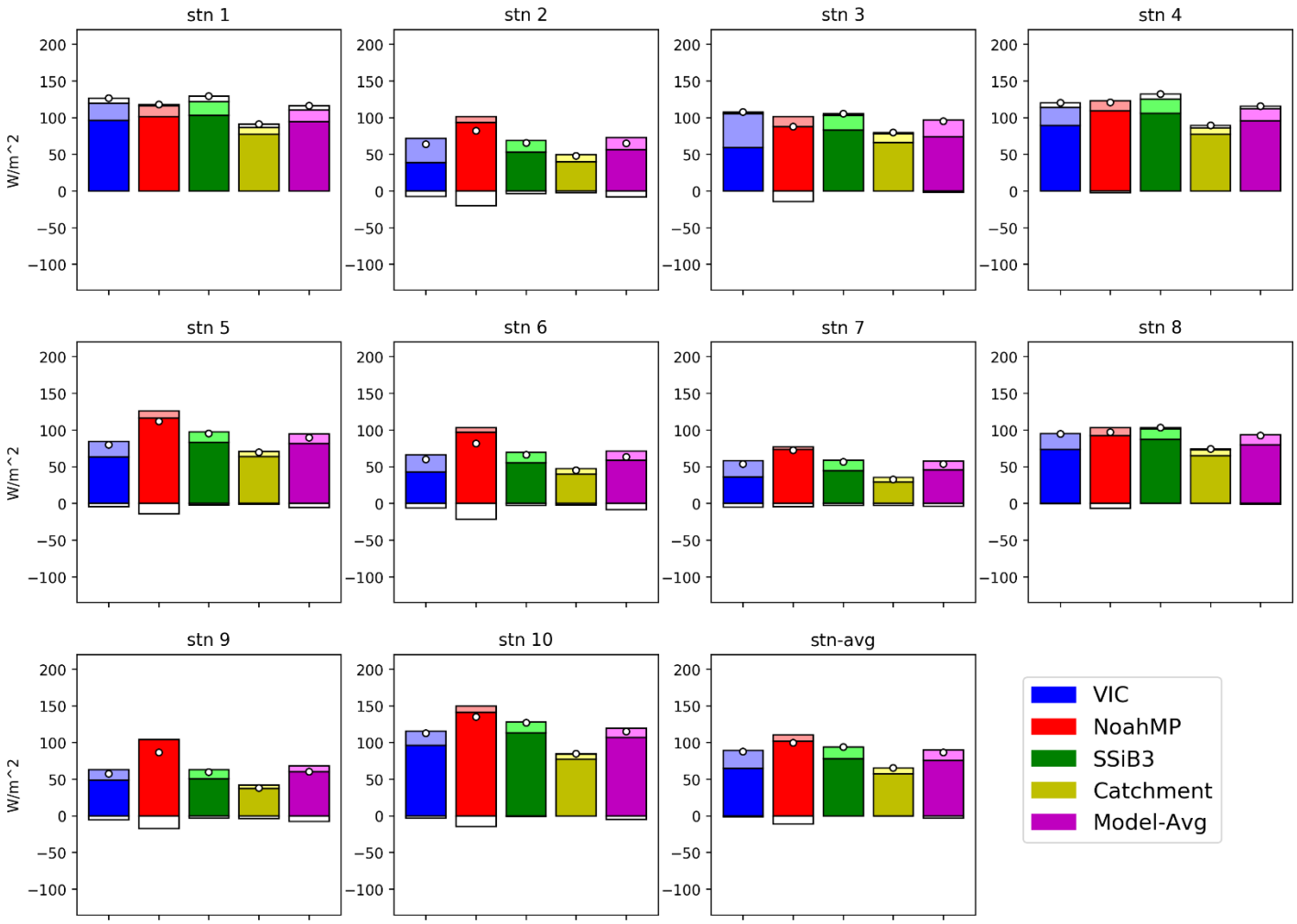

Figure 10: same as Figure 7 but for the no vegetation simulation.

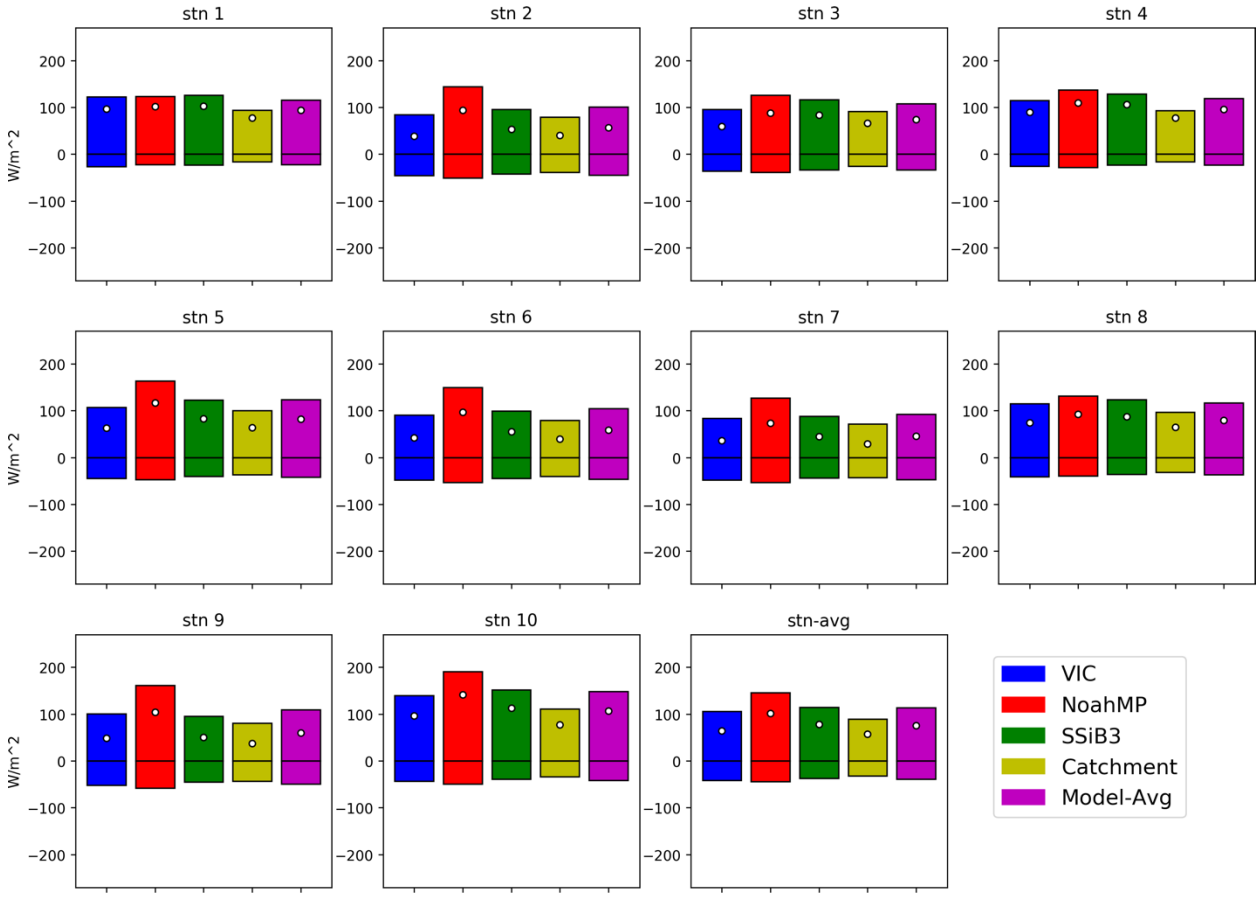

Figure 11: same as Figure 8 but for no vegetation simulation.

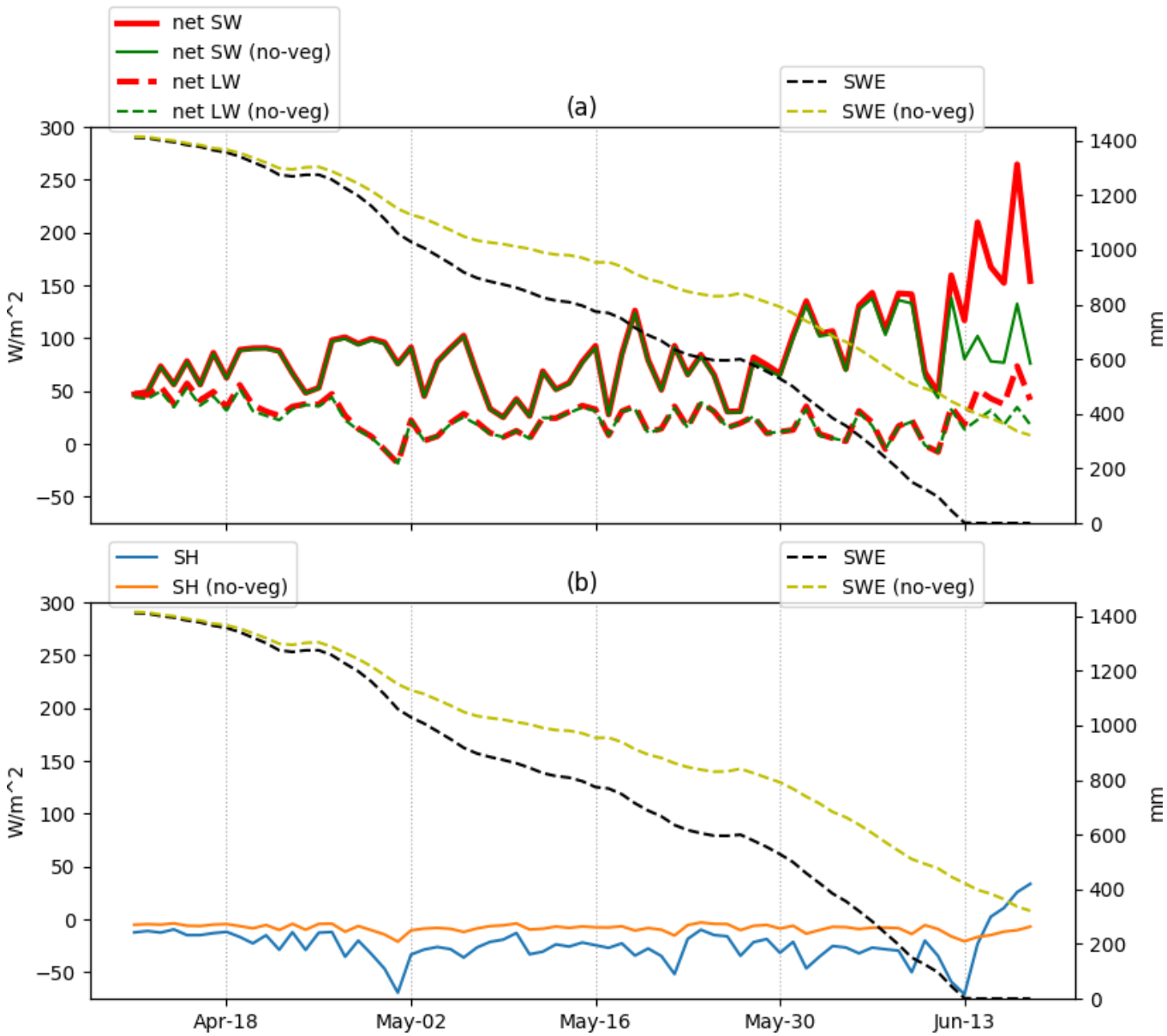

Figure 12: Time-series plot of (a) net shortwave (net SW), net longwave (net LW) and (b) sensible heat (SH) at Olallie Meadows station in 1998 for both baseline and no-veg simulations. The Snow Water Equivalent (SWE) are plotted on a secondary scale in both panels to indicate the ablation season.